Hindawi
Journal of Combustion
Volume 2018, Article ID 6931483, 12 pages
https://doi.org/10.1155/2018/6931483

Research Article

Simulation of Coal and Biomass Cofiring with Different Particle Density and Diameter in Bubbling Fluidized Bed under O_2/CO_2 Atmospheres

Chao Chen,[1] **Xuan Wu**,[1] **and Lingling Zhao**[1,2]

[1]*School of Energy & Environment, Southeast University, Nanjing, Jiangsu 210096, China*
[2]*Key Laboratory of Energy Thermal Conversion and Control of Ministry of Education, Nanjing, Jiangsu 210096, China*

Correspondence should be addressed to Lingling Zhao; zhao_lingling@seu.edu.cn

Received 3 May 2018; Revised 26 July 2018; Accepted 18 August 2018; Published 12 September 2018

Academic Editor: Hiroaki Watanabe

A 2D dynamic model for a bubbling fluidized bed (BFB) combustor has been developed for simulating the coal and biomass cofiring process under 21% O_2/79% CO_2 atmosphere in a 6 kWth bubbling fluidized bed, coupled with the Euler-Euler two-phase flow model. The kinetic theory of binary granular mixtures is employed for the solid phase in order to map the effect of particle size and density. The distribution of temperature, volume fraction, velocity, gas species concentration, and reaction rates are studied with numerical calculations. The simulated temperature distribution along the height of the combustor and outlet gas concentrations show good agreement with experimental data, validating the accuracy and reliability of the developed cofiring simulation model. As indicated in the results, there are two high temperature zones in the combustor, which separately exist at the fuel inlet and dilute phase. The reaction rates are related to the species concentration and temperature. The higher concentration and temperature lead to the larger reaction rates. It can be seen that all of the homogeneous reaction rates are larger at the fuel inlet region because of rich O_2 and volatiles. High mass fraction of volatile gas is found at the fuel inlet, and the main reburning gas at the dilute phase is CH_4. The mass fraction distribution of CO is related to the volume fraction of fuel which is due to the fact that the source of CO is not only from the devolatilization but also from the gasification. On the basis of this theoretical study, a better understanding of flow and combustion characteristics in biomass and coal cofiring under oxy-fuel atmospheres could be achieved.

1. Introduction

Biomass is a carbon-neutral fuel with a large reserve available, producing no net CO_2 emissions in its life cycle, and can reduce net CO_2 emissions effectively in coal-based power plants [1]. Biomass cofiring with coal provides an alternative way to utilize biomass fuel effectively due to its' many advantages such as low risk, good emission properties, and better fuel economy [2, 3]. Fluidized bed (FB) combustion technology is suitable for biomass and coal cocombustion due to its high combustion efficiency for various types of fuel and better emission characteristics [4–6]. What is more, in comparison with pulverized-fuel (PF) boilers, fluidized bed combustors could be designed with a relatively small investment for conversion from coal combustion to biomass and coal cofiring.

Oxy-fuel combustion technology is a type of carbon-capture technology first proposed by Abraham et al. in 1982 [7]. Several experimental investigations demonstrated the potential and economic value of its application in fluidized bed combustors [8–10]. In recent years, researchers have paid more attention to biomass and coal cofiring in oxy-fuel fluidized bed combustors [11]. Tan et al. [12] conducted a series of tests on combustion and emission characteristics of wood cofiring with coal in a pilot-scale oxy-fuel circulating fluidized bed (CFB) combustor and concluded that it is feasible for achieving negative emissions of CO_2. Duan et al. [13] studied NO emission from biomass and coal cofiring in a 10 kWth CFB under oxy-fuel conditions. It was found that the emission of NO in an O_2/CO_2 atmosphere is lower than that in an air atmosphere. Experiments were carried out by Kumar and Singh [14, 15] to investigate the temperature profile,

gas emission, particle size distribution, and combustion efficiency of four kinds of biomass cofiring with coal under an oxy-fuel atmosphere in a 20 kWth CFB.

Computational fluid dynamics (CFD) has been widely used to study the combustion and flow characteristics of biomass cofiring with coal [16–21]. Gungor [22] simulated the biomass and coal cofiring in CFB using a developed model which investigated the effect of biomass fraction on CO, NO_x, and SO_2 emissions. Zhang et al. [23] simulated the combustion of low density biomass (oat hulls) cofiring with coal in a fluidized bed combustor by using an Euler-Lagrange model and found that the mass fraction of biomass can affect the peak temperature of the furnace, while the adjustment of the secondary air can strongly affect the combustion of oat hulls. However, there have been only a few studies in which biomass cofiring in FB was simulated under an oxy-fuel atmosphere. Bhuiyan et al. [24, 25] simulated biomass cofiring in PF under an O_2/CO_2 atmosphere and studied the effects of oxygen concentration and biomass ratio on combustion characteristics.

There are two main approaches to describe the hydrodynamic behavior of particles in the fluidized bed: Lagrange (discrete element) and Eulerian (continuum). The Lagrange approach tracks every individual particle in the random flow field by solving its motion equation. The external force directly acting on each particle is taken into account. On the other hand, the Eulerian approach describes the carrier and the dispersed phase with a set of continuum equations representing conservation of mass, momentum, and energy of either phase within a fixed element volume. In the simulation of a dense fluidized bed, the discrete particles are approximated as continuous phase for describing the gas-particle and particle-particle interaction, which is based on the kinetic theory of granular flow (KTGF). The KTGF is developed from the kinetic theory of dense gases [26]. It is based on the Boltzmann equation, which represents the relative disordered motion of particles according to the collision and fraction through the granular temperature (θ). Goldschmidt et al. [27] demonstrated that simulations using KTGF agree well with the elastic particles model of a fluidized bed. Nevertheless, the original KTGF [28] cannot model a mixture with different size/density particles, due to the assumption that all particles have equal granular temperature [29, 30]. Hence, Lu et al. [30, 31] extended the KTGF model to a binary granular mixture with different granular temperatures by means of the Maxwell distribution. Wang et al. [32] simulated combustion and desulfurization processes in CFB with various particle size/density (coal/limestone) using the KTGF model with different granular temperatures. It is obvious that the flow and combustion characteristics of fuel are greatly affected by the particle size and density [33]. The assumption of average density and particle size limits the accuracy of simulations [21, 32]. Therefore, it is necessary to establish a model of coal and biomass cofiring in FB with different particle size and density.

In this study, the combustion and flow characteristics of biomass cofiring with coal in a 6 kWth oxy-fuel bubbling fluidized bed combustor have been investigated using CFD. The constitutive properties of the dispersed solid phases are predicted with the kinetic theory of binary granular mixtures. The unsteady processes of gas-solid two-phase flow, heat, and mass transfer incorporating the devolatilization, heterogeneous, and homogeneous reactions are considered in this simulation.

2. Computational Modelling

Based on an Euler-Euler approach, a complicated model including gas-solid multiphase flow, interphase heat and mass transfer, devolatilization of coal and biomass, and homogeneous and heterogeneous reactions has been established. In order to ensure the good convergence and acceptable computational time, the established model was simplified; the main assumptions adopted in this study are listed as follows. (1) The mesh model is assumed as 2-dimensional with the furnace depth of 0.05 m. The widths of dilute and dense zones in the 2D case are determined based on the corresponding cross-section area in the 3D furnace. (2) The solid phase is composed of coal and biomass particles with different density and diameter. Both of them are assumed as inelastic spheres. (3) The gas is considered to be incompressible and ideal and there is no slippage near the wall. (4) The intensity of granular collision is independent with bed temperature. (5) The radiant heat transfer in the furnace is ignored, but the wall radiation is taken into account in the overall wall heat transfer coefficient. For good computational convergence, the heat transfer between coal and biomass particles is neglected. (6) Energy transfer induced by the effect of pressure, viscous dissipation, and compositional diffusion is ignored. (7) The reactions of denitration and desulfurization processes are neglected in the combustion submodel due to the less influence on temperature field.

2.1. Hydrodynamic Model

2.1.1. Gas Phase. The governing equations for gas phase are shown as (1)-(3), where the subscripts s and g represent solid phase and gas phase, respectively. α, ρ, $\vec{u}$, p, H, and T are the volume fraction, the density, the instantaneous velocity, the pressure, the enthalpy, and the temperature, respectively. S_g^m is the mass source term for gas phase contributed by chemical reactions. $\overline{\overline{\tau}}$ is the stress-strain tensor. $\beta_{s,g}$ is the gas-solid drag coefficient which is defined as Gidaspow model [47]. $\dot{m}_{s,g}$ means the mass transfer from solid phase to gas phase. $\vec{J}_e$ in (3) is the energy source term, including the heat generation per unit volume and the heat exchange caused by convection between gas and solid. λ is the coefficient of heat transfer between gas and solid calculated by Gunn's model [48]. The species conservation equation is expressed by (4), where subscript i=1-8 representing the 8 kinds of species (H_2O, H_2, CO, CO_2, CH_4, C_2H_6, tar, and O_2) in the gas phase. $Y_{g,i}$ is the mass fraction for gas i, $\vec{J}_i$ is the diffusion flux caused by concentration gradient of species i, and R_i is the substance reaction rates during chemical reactions.

$$\frac{\partial}{\partial t}\left(\alpha_g \rho_g\right) + \nabla \bullet \left(\alpha_g \rho_g \vec{u_g}\right) = S_g^m \tag{1}$$

$$\frac{\partial}{\partial t}\left(\alpha_g \rho_g \overrightarrow{u_g}\right) + \nabla \bullet \left(\alpha_g \rho_g \overrightarrow{u_g}\overrightarrow{u_g}\right) = -\alpha_g \nabla p + \alpha_g \nabla \bullet \overline{\overline{\tau_g}} + \alpha_g \rho_g g + \sum_{i=1} \beta_{s_i g}\left(\overrightarrow{u_{s_1}} - \overrightarrow{u_g}\right) + \sum_{i=1} \dot{m}_{s_i g} \overrightarrow{u_{s_1}} \quad (2)$$

$$\frac{\partial}{\partial t}\left(\alpha_g \rho_g H_g\right) + \nabla \bullet \left(\alpha_g \rho_g \overrightarrow{u_g} H_g\right) = \nabla \bullet \left(\lambda_g \nabla T_g\right) + \overrightarrow{J_e} \quad (3)$$

$$\frac{\partial}{\partial t}\left(\rho \alpha_g Y_{g,i}\right) + \nabla \bullet \left(\rho \alpha_g \overrightarrow{u_g} Y_{g,i}\right) = -\nabla \bullet \overrightarrow{J_i} + R_i \quad (4)$$

2.1.2. Particle Phase. The continuity, momentum, and energy equations of solid phase are shown in (5)-(7). The same characters share the same definitions with the gas phase. $\beta_{s_{ij}}$ is the drag coefficient between different particle phases. Based on KTGF for binary granular mixture model, each particle phase has different size, density, and granular temperature. The kinetic energy equation for particle phases is shown in (8), where θ_i is the granular temperature for each particle phase. k_{θ_i}, γ_{θ_i}, and ϕ_{sg} are the diffusion coefficient for particle phase, the dissipation rate caused by particle inelastic collision, and kinetic energy exchange between gas and particles, respectively. The detailed derivation for KTGF of binary granular mixture model is given in [30, 32] .

$$\frac{\partial}{\partial t}\left(\alpha_{s_i} \rho_{s_i}\right) + \nabla \bullet \left(\alpha_{s_i} \rho_{s_i} \overrightarrow{u_{s_i}}\right) = S_{s_i}^m \quad (5)$$

$$\frac{\partial}{\partial t}\left(\alpha_{s_i} \rho_{s_i} \overrightarrow{u_{s_i}}\right) + \nabla \bullet \left(\alpha_{s_i} \rho_{s_i} \overrightarrow{u_{s_i}}\overrightarrow{u_{s_i}}\right) = -\alpha_{s_i} \nabla p + \alpha_{s_i} \nabla \bullet \overline{\overline{\tau_{s_i}}} + \alpha_{s_i} \rho_{s_i} g - \beta_{s_i g}\left(\overrightarrow{u_{s_i}} - \overrightarrow{u_g}\right) + \sum_{i=1, i\neq j} \beta_{s_{ij}}\left(\overrightarrow{u_{s_i}} - \overrightarrow{u_{s_j}}\right) - \sum_{i=1} \dot{m}_{s_i g} \overrightarrow{u_{s_i}} \quad (6)$$

$$\frac{\partial}{\partial t}\left(\alpha_{s_i} \rho_{s_i} H_{s_i}\right) + \nabla \bullet \left(\alpha_{s_i} \rho_{s_i} \overrightarrow{u_{s_i}} H_{s_i}\right) = \nabla \bullet \left(\lambda_{s_i} \nabla T_{s_i}\right) + \overrightarrow{J_e} \quad (7)$$

$$\frac{3}{2}\left[\frac{\partial}{\partial t}\left(\alpha_s \rho_s \theta_i\right) + \nabla \bullet \left(\alpha_s \rho_s \theta_i \overrightarrow{u_i}\right)\right] = \overline{\overline{\tau_{s_i}}} : \nabla \overrightarrow{u_i} + \nabla \bullet \left(k_{\theta_i} \nabla \theta_i\right) - \gamma_{\theta_i} + \phi_{sg} \quad (8)$$

2.2. Chemical Reaction Model. The cofiring process of coal and biomass is defined as 3 parts: water evaporation and devolatilization, homogeneous reactions (volatile combustion), and heterogeneous reactions (char oxidation and gasification). All of the reaction rates are shown in Table 1.

2.2.1. Coal and Biomass Devolatilization Model. Five volatile products are considered during coal and biomass devolatilization: CH_4, H_2, CO, tar, and C_2H_6 [40, 49, 50]. The devolatilization of coal and biomass is expressed by reaction (R1). Y_c and Y_v are the mass fractions of char and volatile, respectively. The amount of volatile products is calculated by the correlation used in [40, 51].

$$\text{1kg dry fuel} \longrightarrow Y_c \text{ kg char} + Y_v \text{ kg volatile} + \left(1 - Y_c - Y_v\right) \text{kg ash} \quad (R1)$$

2.2.2. Homogeneous and Heterogeneous Reactions. Reactions (R2)-(R6) are the homogeneous reactions. The combustion rates of volatiles follow Arrhenius's law. The char oxidation and gasification reactions are shown in (R7)-(R9), where ϕ is mechanical factor determining the balance of CO and CO_2 production.

$$CH_4 + 1.5O_2 \longrightarrow CO + 2H_2 \quad (R2)$$

$$CO + 0.5O_2 \longrightarrow CO_2 \quad (R3)$$

$$H_2 + 0.5O_2 \longrightarrow H_2O \quad (R4)$$

$$CH_aO_b + \frac{(2+a)}{(2-b)}O_2 \longrightarrow CO_2 + \left(\frac{a}{2}\right)H_2 \quad (R5)$$

$$C_2H_6 + 2.5O_2 \longrightarrow 2CO + 3H_2O \quad (R6)$$

$$C + \left(\frac{1}{\phi}\right)O_2 \longrightarrow \left(2 - \frac{2}{\phi}\right)CO + \left(\frac{2}{\phi} - 1\right)CO_2 \quad (R7)$$

$$C + CO_2 \longrightarrow 2CO \quad (R8)$$

$$C + 1.2H_2O \longrightarrow 1.2H_2 + 0.2CO_2 + 0.8CO \quad (R9)$$

2.3. Numerical Method and Boundary Conditions. A 2D mesh was established to simulate the furnace of the bubbling fluidized bed which is shown in Figure 1. As shown in the figure, the fuel inlet, secondary air inlet, and the fuel gas outlet are at the heights of 0.18 m, 0.65 m, and 1.5 m, respectively. The grids at the fuel inlet and the secondary air inlet were refined. The total number of girds is 7751. Some main parameters used in the simulation are shown in Table 2. The selection of restitution coefficients is referred from [32, 52, 53]. The proximate analysis and ultimate analysis of coal and biomass (woodchips) are shown in Table 3.

Fluent software was used in this study, and unsteady equation was employed in the solution. Pressure-temperature coupling employed SIMPLE algorithm, and gradient interpolation employed Green-Gauss algorithm based on elementary volume. Velocity of the solid phase was assumed to be 0 at the initial time, and velocity of the gas phase was the same as the inlet velocity of primary air. Temperature in the furnace was uniform. Mirror coefficient of solid particle was considered to be 0.5 and thickness of the wall was 0.2 m. The chemical reaction rates coupled with the model were determined by user-defined functions. No slip boundary condition was applied for gas phase and Johnson-Jackson model [54] was adopted for particle phases at near wall region.

Table 1: Rates for the homogeneous and heterogeneous reactions.

	Reaction rate r/kmol.m^{-3}s^{-1}	Reaction coefficient k_c
	Coal and biomass devolatilization	
(R1)	$r_1 = \alpha_{s_i} k_1 C_{rawc}$ [34, 35]	$k_1 = \begin{cases} 4.136 \times 10^4 (\mathrm{s}^{-1}) \exp(-0.73 \times 10^8 / RT) & \text{coal} \\ 9.2 \times 10^8 (\mathrm{s}^{-1}) \exp(-1.3576 \times 10^8 / RT) & \text{biomass} \end{cases}$
	Homogeneous reactions	
(R2)	$r_2 = \alpha_g k_2 C_{O_2}^{0.8} C_{CH_4}^{0.7}$ [36]	$k_2 = 5.0122 \times 10^{11} (\mathrm{m}^{1.5}\mathrm{kmol}^{-0.5}\mathrm{s}^{-1}) \exp(-2.0085 \times 10^8 / RT)$
(R3)	$r_3 = \alpha_g k_3 C_{CO} C_{O_2}^{0.5} C_{H_2O}^{0.5}$ [37]	$k_3 = 1.3 \times 10^{11} (\mathrm{m}^3\mathrm{kmol}^{-1}\mathrm{s}^{-1}) \exp(-1.255 \times 10^8 / RT)$
(R4)	$r_4 = \alpha_g k_4 C_{O_2} C_{H_2}$ [38]	$k_4 = 1.0 \times 10^8 (\mathrm{m}^3\mathrm{kmol}^{-1}\mathrm{s}^{-1}) \exp(-0.083 \times 10^8 / RT)$
(R5)	$r_5 = \alpha_g k_5 C_{O_2} C_{tar}$ [39]	$k_5 = 3.8 \times 10^7 (\mathrm{m}^3\mathrm{kmol}^{-1}\mathrm{s}^{-1}) \exp(-0.555 \times 10^8 / RT)$
(R6)	$r_6 = \alpha_g k_6 C_{C_2H_6} C_{O_2}$ [40]	$k_6 = 1.068 \times 10^5 (\mathrm{m}^3\mathrm{kmol}^{-1}\mathrm{s}^{-1}) T^{0.5} \exp(-1.674 \times 10^8 / RT)$
	Heterogeneous reactions	
(R7)	$r_7 = (6\alpha_{s_i}\rho_{s_i} Y_{char} / d_{s_i}\rho_c) \bullet k_c C_{O_2} k_7$ $k_c = (RT/w_c)/(1/k_d + 1/k_7)$ [40–42]	$k_7 = 8910 (\mathrm{kgm}^3\mathrm{s}^{-1}\mathrm{kPa}^{-1}) \exp(-1.4974 \times 10^8 / RT)$, $k_d = \phi Sh D_g w_c / d_{s_i} RT_g$, $Sh = 2\varepsilon + 0.69 (Re/\varepsilon)^{1/2} Sc^{1/3}$, $Re = u d_p \rho_g / \mu_g$ $Sc = \mu_g / \rho_g D_g$, $D_g = D_{g_0} \bullet (T/T_0)^{1.75} (p/p_0)$, $D_{g_0} = 3.13 \times 10^{-4} (\mathrm{m}^2\mathrm{s}^{-1})$, $T_0 = 1500(\mathrm{K})$, $p_0 = 101325(\mathrm{Pa})$
(R8)	$r_8 = k_8 C_{CO_2} / (1 + K^8_{k_{co_2}} C_{CO_2} + K^8_{k_{co}} C_{CO})$ [43–45]	$k_8 = 4.89 \times 10^{10} (\mathrm{m}^3\mathrm{kmol}^{-1}\mathrm{s}^{-1}) \exp(-2.68 \times 10^8 / RT) (\rho_s Y_c / MW_s)(1 - X)$, $K^8_{k_{co_2}} = 66 (\mathrm{m}^3\mathrm{kmol}^{-1})$, $X = 0.35$, $K^8_{k_{co}} = 1.20 \times 10^2 (\mathrm{m}^3\mathrm{kmol}^{-1}) \exp(-2.55 \times 10^7 / RT)$,
(R9)	$r_9 = k_9 C_{H_2O} / (1 + K^9_{k_{H_2O}} C_{H_2O2} + K^9_{k_{H_2}} C_{H_2} + K^9_{k_{CO}} C_{CO})$ [43, 46]	$k_9 = 2.39 \times 10^5 (\mathrm{m}^3\mathrm{kmol}^{-1}\mathrm{s}^{-1}) \exp(-1.29 \times 10^{-8} / RT) (\rho_s Y_s / MW_c)(1 - X)$ $K^9_{k_{H_2O}} = 31.6 (\mathrm{m}^3\mathrm{kmol}^{-1}) \exp(-3.01 \times 10^7 / RT)$, X = 0.5, $K^9_{k_{H_2}} = 5.36 (\mathrm{m}^3\mathrm{kmol}^{-1}) \exp(-5.98 \times 10^7 / RT)$, $K^9_{k_{CO}} = 8.25 \times 10^{-2} (m^3 kmol^{-1}) \exp(-9.61 \times 10^7 / RT)$

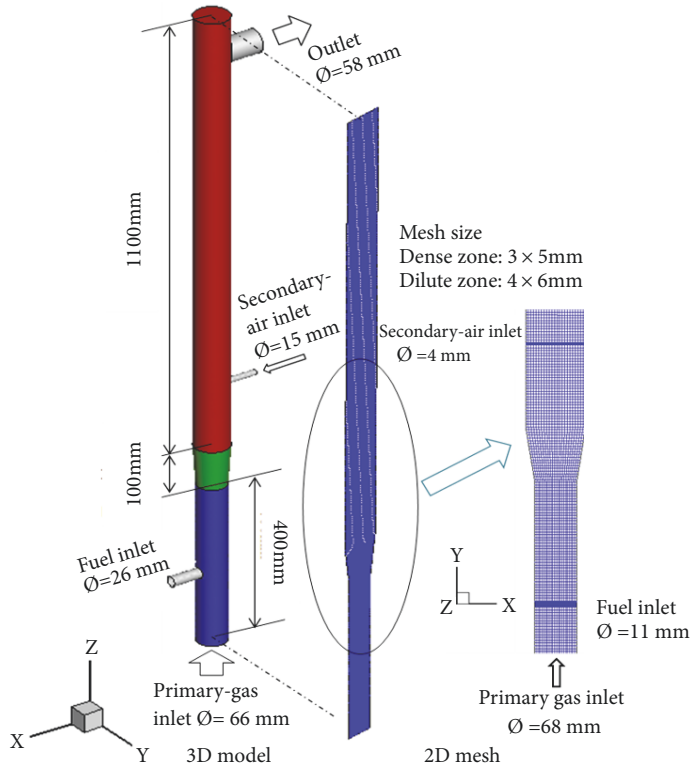

Figure 1: Schematics of the combustor and simulation grids.

Table 2: Parameters used in the simulation.

Parameters	value
Diameter of coal	0.7 mm
Diameter of biomass	0.9 mm
Density of coal	1280 kg/m^3
Density of biomass	600 kg/m^3
Density of ash	2200 kg/m^3
Fuel feed rate	0.87 kg/h
Restitution coefficient between different particles	0.95
Restitution coefficient between same particles	0.9
O_2/CO_2 volume fraction	21%/79%
Excess O_2 coefficient[a]	1.14
Primary air/ secondary air volume fraction	81%/19%
Gas phase inlet temperature	423 K
Fuel inlet temperature	300 K
Wall temperature	700 K
Velocity of primary air	0.512 m/s
Velocity of secondary air	2.04 m/s
Initial bed height	0.4 m
Initial bed temperature	1123 K

a: the oxygen/fuel ratio normalized by the actual stoichiometric oxygen/fuel ratio.

Table 3: Fuel ultimate analysis and proximate analysis.

Fuel Name	Coal	Biomass
Ultimate analysis/wt.%		
C_{ad}	67.42	46.99
H_{ad}	4.14	5.75
O_{ad}	7.98	39.86
N_{ad}	1.04	0.39
S_{ad}	2.72	0.11
LHV MJ/kg	26.60	17.086
Proximate analysis/wt.%		
FC_{ad}	48.30	17.59
V_{ad}	35.00	75.51
A_{ad}	9.9	3.34
M_{ad}	6.8	3.36

The simulation was conducted for 30 s with the time step being set as 1×10^{-4} s. For the first 0.1 s, gas-ash fluidization was simulated at temperature of 1123 K without fuel feeding, and then coal and biomass were continuously fed into the furnace.

3. Results and Discussion

3.1. Validation. In order to get reliable statistics of combustion characteristics in the fluidized bed, the volume fractions of three gas species (CO_2, O_2, and H_2O) at gas outlet are monitored. The results are shown in Figure 2. It can be seen that the average volume fractions of CO_2 and H_2O at the

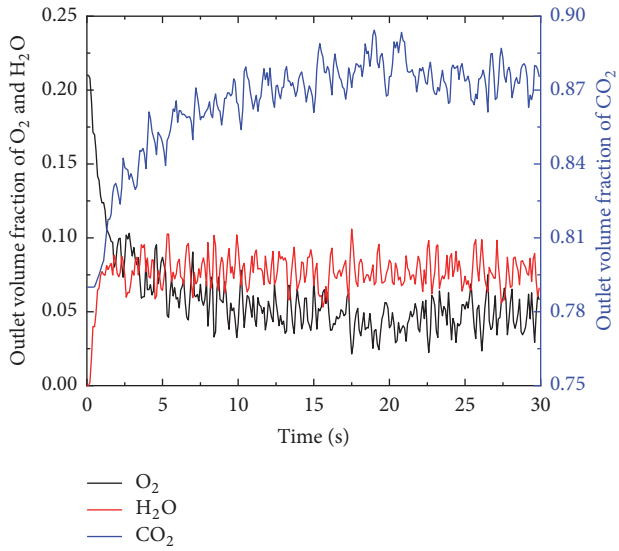

FIGURE 2: The gas (CO_2, O_2, and H_2O) volume fractions along with time at the outlet.

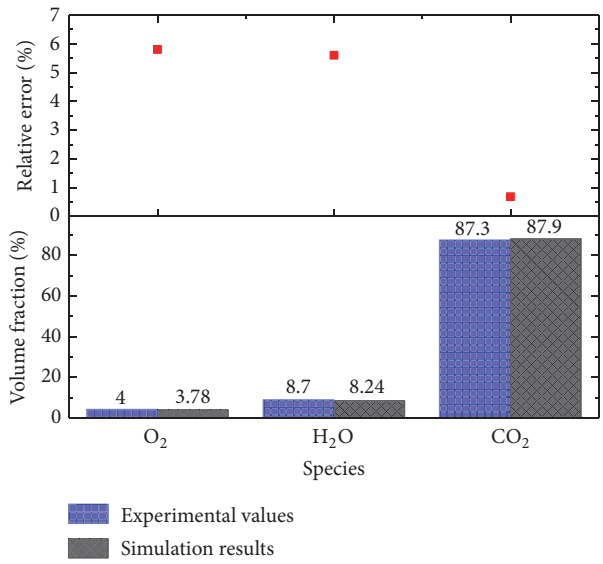

FIGURE 3: The experimental and simulation results of the outlet gas volume fractions.

outlet gradually increased form 79% to 86.42% and 0% to 9.36%, respectively, during the initial 10 s. At the same time, the volume fraction of O_2 decreased from 21% to 4.18%. However, the volume fractions for the CO_2, O_2, and H_2O are relatively stable after 15 s of simulation, which fluctuate around 87.8%, 4.54%, and 7.55%. Therefore, the 20-30 s time-averaged calculation results are adopted to analyze the flow and combustion characteristics in this paper.

To demonstrate the accuracy of the simulation results, the experiment of 6 kWth bubbling fluidized bed under 21% O_2/79% CO_2 atmosphere had been conducted at Southeast University, Nanjing, China [54]. Figure 3 shows the experimental and simulation values of CO_2, O_2, and H_2O volume fractions at the outlet. The relative errors of volume fractions of O_2, H_2O, and CO_2 are 5.8%, 5.6%, and 0.682%, respectively. The simulation values are in good agreement with the experimental results.

3.2. Flow Characteristic. Figure 4 shows the instantaneous volume fractions of coal and biomass under the conditions of primary air velocity, fuel feed rate, and biomass/coal mass ratio of 0.71 m/s, 0.87 kg/h, and 0.25, respectively. The volume fractions for coal and biomass phase are both 0.275 at the initial time. The coal and biomass entered the riser from the fuel inlet which is at the height of 0.18 m. It can be seen that the cluster of biomass and coal is formed at the fuel inlet (at 19.6 s) and falls down along the wall to the bottom of the riser and then rises up due to the primary air (from 19.8 s to 20.4 s). The formation of bubble can be observed while the primary air is rising. The bubbles grow, change the shapes, split, and combine along with the time building up. At last, the bubble breaks up above the secondary air inlet. The bubbling fluidization can be observed obviously in the figure of the instantaneous volume fraction distribution of coal and biomass.

The time and section-averaged volume fraction and pressure distribution along the axial height are shown in Figure 5. The volume fraction of coal is higher than that of biomass at the bottom of riser. The coal particles suffer greater gravity force due to the larger density, which lead to the more deposition of coal at the bottom of riser. However, the volume fraction of biomass is higher than biomass when the height is over 0.2 m. In comparison with Figure 4, it indicates that the biomass particles are more likely to rise up along with the primary air. The bed pressure distribution is also shown in Figure 5. The maximum of bed pressure is 2280 Pa. The bed pressure decreases along the axial height of the bed, which is maintained at -50 Pa when the height is higher than 0.8 m. The riser is divided into three zones which is dense zone (0-0.5 m), transition zone (0.5-0.8 m), and dilute zone (0.8-1.6 m), respectively.

Figure 6 shows the time-averaged axial velocity distribution of coal, biomass, and gas at heights of 0.05 m, 0.45 m, and 0.7 m. Combined with Figure 4, it can be seen that the velocity of gas phase is larger at the center due to the lower volume fraction of particles. The coal and biomass particles rise with the gas due to the effect of gas drag at the center. However, the volume fractions of coal and biomass are so high at the near wall region that the gas drag is not larger enough to carry the coal and biomass particles there. In that case, the velocities at the near wall region are negative which means the falling of particles. Comparing the velocities between the biomass and coal particles, the rise velocity of coal particles is lower than that of biomass particles. Consequently, the coal and biomass particles with low volume fraction flow up at the center and flow down with high volume fraction near the wall. In the rise reactor, the internal circulation of particle flow can be observed.

3.3. Temperature Profile. Figure 7 displays the section- and time-averaged simulation temperature during 20~30 s along the axial height of the riser and the experimental temperature values. The experimental values at 4 height points (0.16 m,

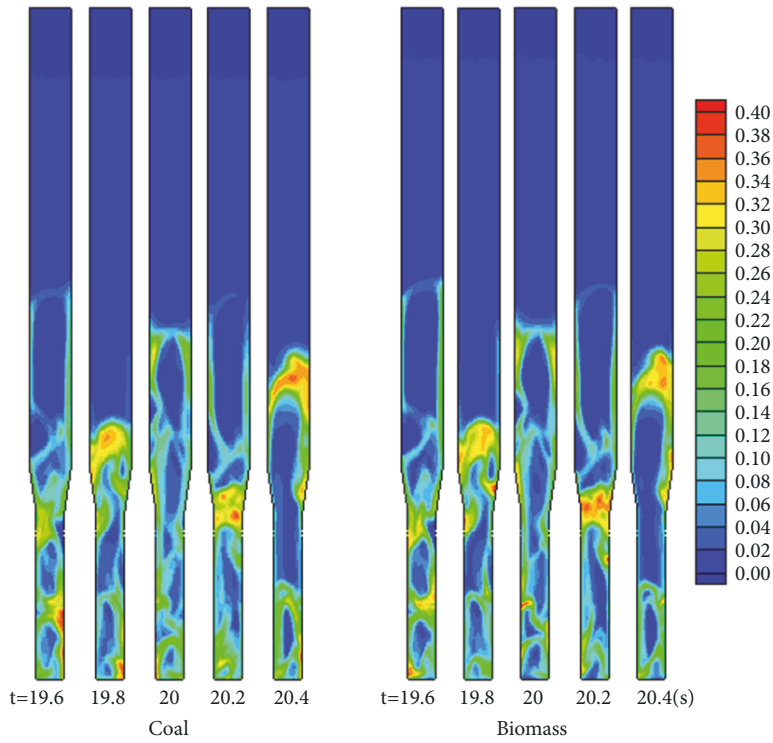

Figure 4: The instantaneous volume fraction of coal and biomass.

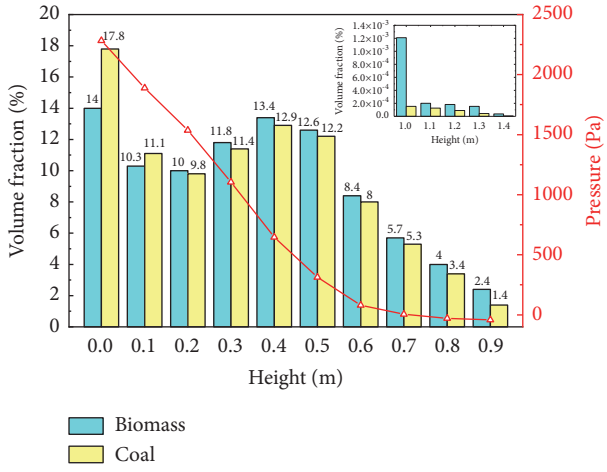

Figure 5: The time- and section-averaged volume fraction of coal and biomass along the height.

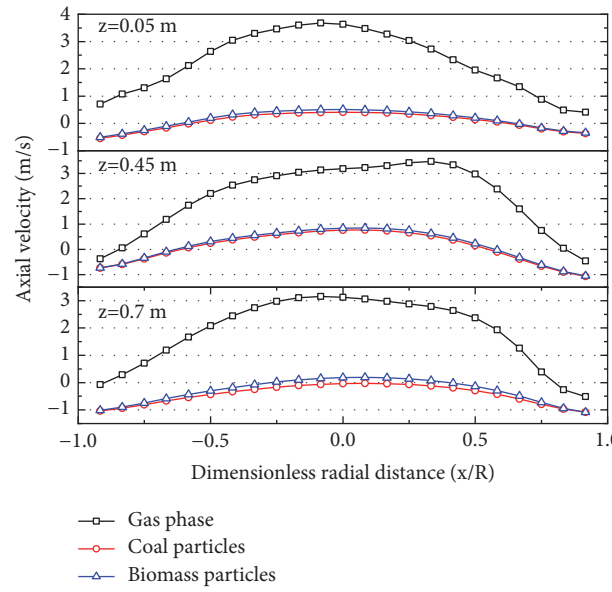

Figure 6: The axial velocity profile of coal, biomass, and gas phase (m/s).

0.29 m, 0.8 m, and 1.2 m) are 1065 K, 1097 K, 1082 K, and 1033 K, respectively. The relative errors between the experimental value and the simulation temperature are separately 1.29%, 0.09%, 1.64%, and 3.82%. The larger relative error at 1.2 m may be due to the higher radial temperature gradient caused by the secondary air. Nevertheless, all of the temperature relative errors are less than 5%, which also indicated the accuracy of the established models in this work.

Figure 8 shows the instantaneous temperature distribution in the furnace. A high temperature region is observed above the fuel inlet (0.2~0.3 m) where temperature is about 1100~1200 K. This is due to the combustion of the volatiles which are released from the coal and biomass. In fact, combining with Figure 7, it can be seen that there is a low temperature region below the fuel inlet (0.16~0.18 m). The reason for this is that the heat is absorbed by the water evaporation and devolatilization of coal and biomass. The

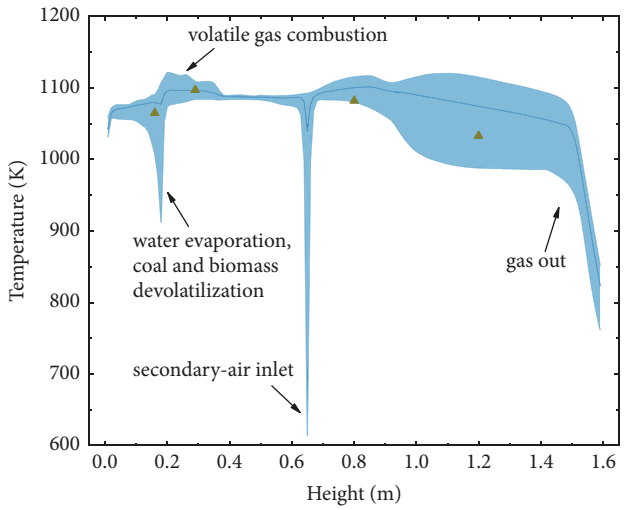

FIGURE 7: The curve: time- and section-averaged temperature of gas and the shadow region: time-averaged temperature range along the axial height.

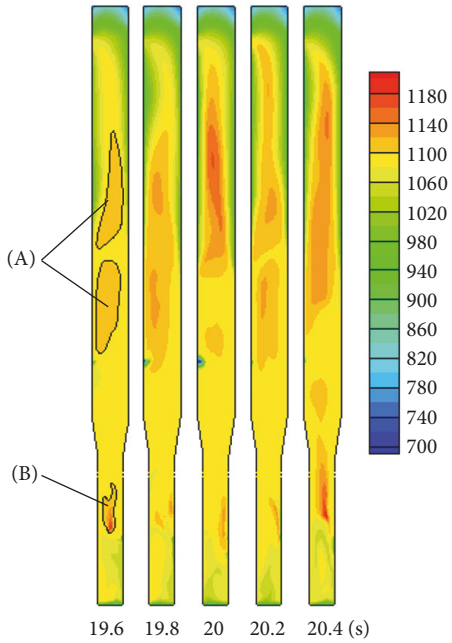

FIGURE 8: The contours of the instantaneous temperature distribution of gas during 19.5-20.5 s (K). Region (A): the high temperature region above the secondary air inlet due to the volatile reburning. Region (B): the high temperature region above the fuel inlet due to the volatile combustion.

average bed temperature at dense zone (0~0.5 m) is 1082 K. The temperature of transition zone (0.5~0.8 m) is uniform whose section-averaged temperature is about 1080 K. It is obvious that the temperature of gas increased again above the secondary air inlet. The cold secondary air (423 K) enters the riser which makes the volatiles reburn. Therefore, the temperature at the center is about 80 K higher than that near wall region.

3.4. Reaction Rates. Figure 9 displays the time-averaged devolatilization rates of biomass and coal. It can be seen that both coal and biomass release the volatile as soon as they enter the riser. The devolatilization rates of them are much higher than other heterogeneous reaction rates. The maximum values of coal and biomass are 0.00374 s^{-1} and 0.01495 s^{-1}. The devolatilization rate of coal is lower than that of biomass. Additionally, the mass fraction of coal is higher. In that case, the devolatilization process of coal lasts to the bottom of the riser, and the devolatilization process of biomass is nearly complete at the fuel inlet.

The homogeneous reaction rates (CH_4, CO, tar, and H_2) are shown in Figure 10. The reaction rates are related to the species concentration and temperature. The higher concentration and temperature lead to the larger reaction rates. It can be seen that all of the homogeneous reaction rates are larger at the fuel inlet region because of rich O_2 and volatiles. In that case, most of the volatiles are consumed in the dense zone. The reaction rates decrease with the reduction of volatile and O_2 along the axial height. In fact, the H_2 reaction (R4) only occurs at the fuel inlet due to the higher reaction rate making H_2 being consumed completely in this region. However, the CH_4 and CO are not consumed completely in dense zone. The reburning of them occurs at the secondary air inlet due to the injection of O_2. Consequently, the homogeneous reactions mainly occur in the dense zone.

3.5. Concentration of Gas Species. Figure 11 shows the contours of the instantaneous mass fractions of CH_4, CO, and tar at around 20 s and the maximum values of them are 0.0418, 0.1785, and 0.1214, respectively. It can be found that the mass fractions of CH_4 and tar are high at the fuel inlet region because of the fuel devolatilization and the mass fraction of CO is high in the whole dense zone which may be due to the devolatilization and heterogeneous reactions process. Then, the mass fractions of them gradually drop with the height increase because of the homogeneous reactions. Actually, it is obvious that the CH_4 has not been completely consumed in the riser. In contrast, the tar has been completely consumed after the secondary air inlet. To combine with Figure 4, we can see that the mass fraction distribution of CO is related to the volume fraction of fuel which is due to the fact that the source of CO is not only from the devolatilization but also from the heterogeneous reactions.

Figure 12 displays the time- and section-averaged mass fraction distributions of H_2O, CO_2, and O_2 along the axial height. As shown in Figure 12, we can see that the mass fraction of O_2 decreases rapidly from 16% to 3% in the dense zone (0~0.5 m) because of char and volatile combustion. The mass fraction of H_2O increases at the fuel inlet due to the chemical reaction and water evaporation. The mass fraction of CO_2 increases firstly at the bottom of riser because of the char combustion. The reduction of CO_2 at the fuel inlet is due to the heterogeneous reaction (R8) and the injection of primary air. Then, the volatile combustion leads to the rapid increase of CO_2 mass fraction. The mass fractions of CO_2, H_2O, and O_2 are relatively uniform in the dilute zone.

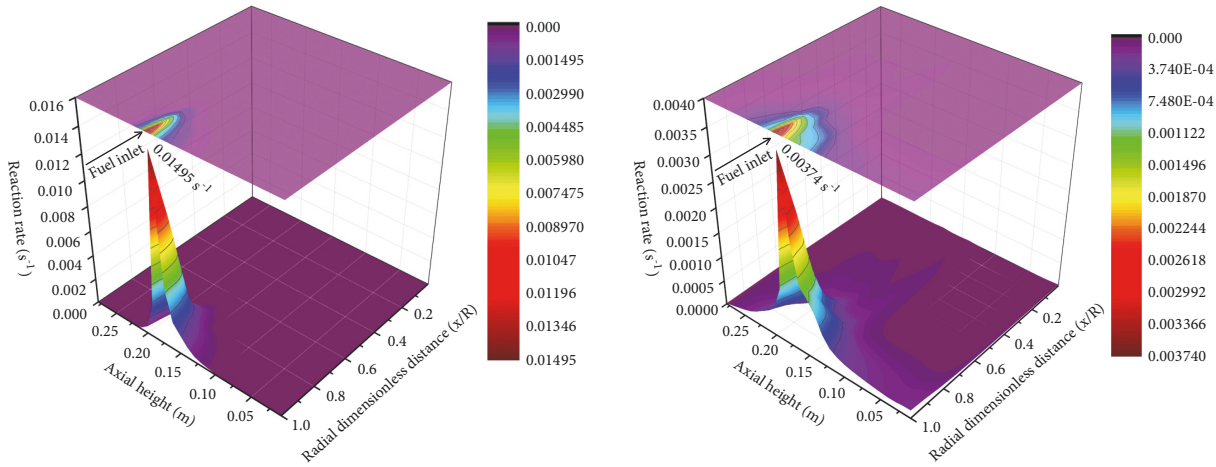

FIGURE 9: Coal (right) and biomass (left) devolatilization rates at fuel inlet region (s^{-1}).

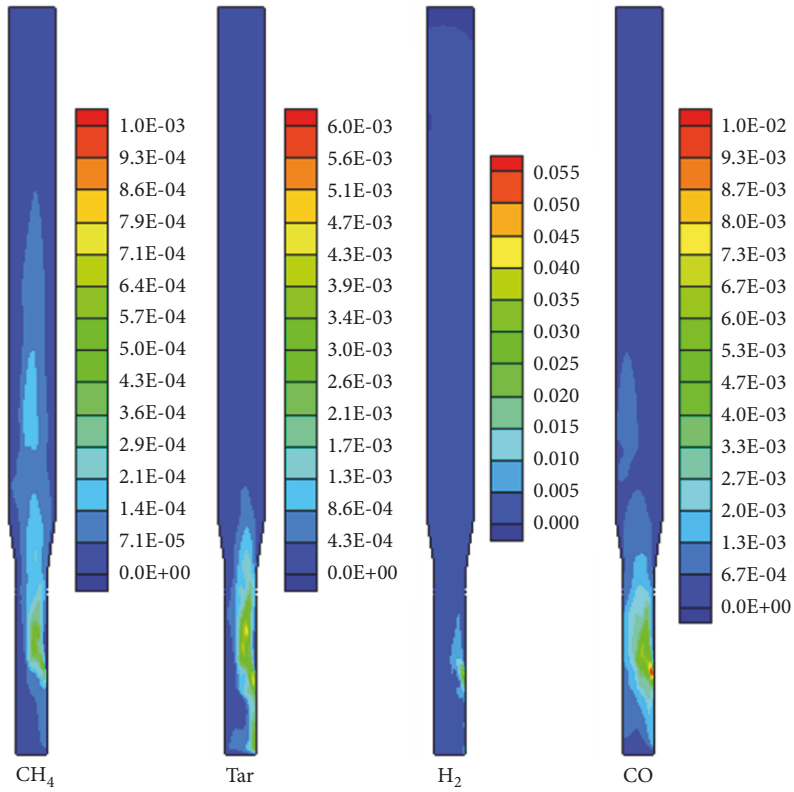

FIGURE 10: Time-averaged homogeneous reaction rates (CH_4, CO, tar, and H_2) (kmol/m^3·s).

4. Conclusion

Based on an Euler-Euler approach, a complicated model including gas-solid multiphase flow, interphase heat and mass transfer, devolatilization of coal and biomass, and homogeneous and heterogeneous reactions has been established to investigate the combustion and flow characteristics of biomass cofiring with coal in a 6 kWth bubbling fluidized bed combustor under 21% O_2/79% CO_2 atmosphere. The simulation values of CO_2, O_2, and H_2O volume fractions at the outlet and temperature distribution along the height of the furnace were satisfactorily validated by the experimental data with no more than 6% relative errors. The results indicated the accuracy of the established models in this work.

The result shows that the bubbling fluidization can be observed obviously in the figure of the instantaneous volume fraction distribution of coal and biomass. During the simulation, two high temperature zones can be found in the rise reactor, which exist at the fuel inlet and dilute phase, respectively. One high temperature region is observed above the fuel inlet (0.18 m) where temperature is about 1100~1200 K. This is due to the combustion of the volatiles

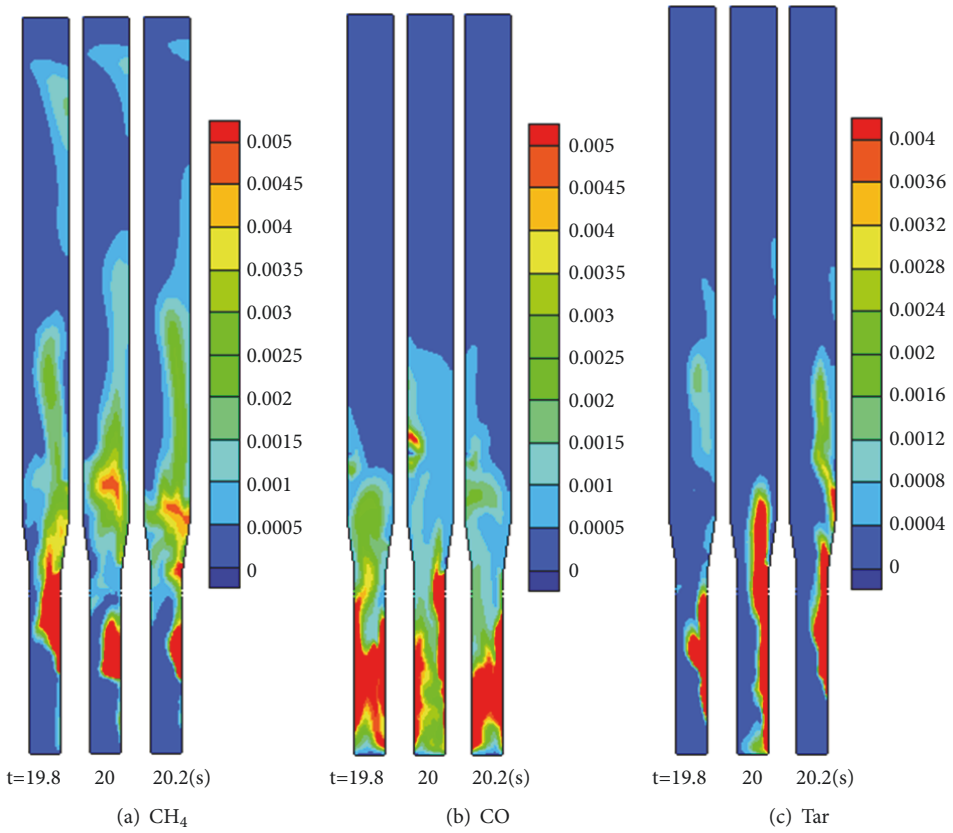

Figure 11: The contours of the instantaneous mass fractions of the main volatile species.

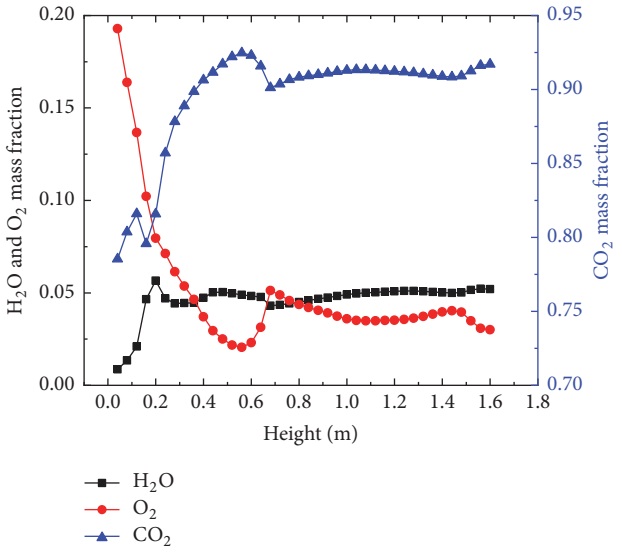

Figure 12: The time- and section-averaged mass fractions of H_2O, O_2, and CO_2 along the height.

which are released from the coal and biomass. The other one is observed above the secondary air inlet (0.65 m). The cold secondary air (423 K) enters the riser which makes the volatiles reburn. Therefore, the temperature at the center is about 80 K higher than that near wall region. It also can be seen that both coal and biomass release the volatile as soon as they enter the riser. The devolatilization rate of coal is lower than that of biomass. As the results indicated, all of the homogeneous reaction rates are larger at the fuel inlet region because of rich O_2 and volatiles and most of the volatiles are consumed in the dense zone. The reaction rates decrease with the reduction of volatile and O_2 along the axial height. High mass fraction of volatile gas (CH_4, CO, etc.) is found at the fuel inlet, and the main reburning gas at the dilute phase is CH_4. The mass fraction distribution of CO is related to the volume fraction of fuel which indicated that the source of CO is not only from the devolatilization but also from the heterogeneous reactions.

Actually, the detailed analysis and modelling of biomass cofiring under O_2/CO_2 atmosphere are extremely complex. On the basis of this theoretical study, a deeper insight of multiphase flow, heat and mass transfer, devolatilization, and homogeneous and heterogeneous reactions during coal and biomass cofiring under O_2/CO_2 atmosphere could be achieved. Certainly, the successful implementation of this technology still requires further study and full understanding of the characteristics of coal and biomass O_2/CO_2 cocombustion in the future.

Data Availability

The simulation and experimental data used to support the findings of this study are available from the corresponding author upon request.

Conflicts of Interest

The authors declare that there are no conflicts of interest regarding the publication of this paper.

Acknowledgments

The authors would like to acknowledge the National Natural Science Foundation of China (51376045) and Postgraduate Research & Practice Innovation Program of Jiangsu Province (KYCX18_0084) for financial support.

References

[1] M. Parikka, "Global biomass fuel resources," *Biomass & Bioenergy*, vol. 27, no. 6, pp. 613–620, 2004.

[2] K. R. G. Hein and J. M. Bemtgen, "EU clean coal technology - Co-combustion of coal and biomass," *Fuel Processing Technology*, vol. 54, no. 1-3, pp. 159–169, 1998.

[3] M. Pronobis, "The influence of biomass co-combustion on boiler fouling and efficiency," *Fuel*, vol. 85, no. 4, pp. 474–480, 2006.

[4] J. Dai, S. Sokhansanj, J. R. Grace, X. Bi, C. J. Lim, and S. Melin, "Overview and some issues related to co-firing biomass and coal," *The Canadian Journal of Chemical Engineering*, vol. 86, no. 3, pp. 367–386, 2008.

[5] M. Akram, C. K. Tan, D. R. Garwood, M. Fisher, D. R. Gent, and W. G. Kaye, "Co-firing of pressed sugar beet pulp with coal in a laboratory-scale fluidised bed combustor," *Applied Energy*, vol. 139, pp. 1–8, 2015.

[6] K. Veijonen, P. Vainikka, T. Järvinen, and E. Alakangas, "Biomass co-firingan efficient way to reduce greenhouse gas emissions," *VTT Processes, March*, p. A1, 2003.

[7] B. M. Abraham, J. G. Asbury, E. P. Lynch, and A. P. S. Teotia, "Coal-oxygen process provides CO_2 for enhanced recovery," *Oil & Gas Journal*, 1982.

[8] E. J. Anthony and H. Hack, "Oxy-fuel combustion on circulating fluidized bed (CFB)," *Oxy-Fuel Combustion for Power Generation and Carbon Dioxide (CO_2) Capture*, vol. 3, pp. 77–98, 2011.

[9] C. S. Zhao, L. B. Duan, X. P. Chen, and C. Liang, *Latest Evolution of Oxy-Fuel Combustion Technology in Circulating Fluidized Bed*, Springer Berlin Heidelberg, 2009.

[10] R. I. Singh and R. Kumar, "Current status and experimental investigation of oxy-fired fluidized bed," *Renewable & Sustainable Energy Reviews*, vol. 61, pp. 398–420, 2016.

[11] S. C. Pickard, S. S. Daood, M. Pourkashanian, and W. Nimmo, "Co-firing coal with biomass in oxygen- and carbon dioxide-enriched atmospheres for CCS applications," *Fuel*, vol. 137, pp. 185–192, 2014.

[12] Y. Tan, L. Jia, and Y. Wu, "Some combustion characteristics of biomass and coal cofiring under oxy-fuel conditions in a pilot-scale circulating fluidized combustor," *ENERGY & FUELS*, vol. 27, no. 11, pp. 7000–7007, 2013.

[13] L. Duan, Y. Duan, C. Zhao, and E. J. Anthony, "NO emission during co-firing coal and biomass in an oxy-fuel circulating fluidized bed combustor," *Fuel*, vol. 150, pp. 8–13, 2015.

[14] R. Kumar and R. I. Singh, "Co-firing of coal with pine needles in a 20 kW oxy-fired bubbling fluidized bed," in *Experimental investigation, Icaer*, pp. 1–6, 2015.

[15] R. Kumar and R. I. Singh, "An investigation in 20 kWth oxygen-enriched bubbling fluidized bed combustor using coal and biomass," *Fuel Processing Technology*, vol. 148, pp. 256–268, 2016.

[16] A. A. Bhuiyan and J. Naser, "Numerical modeling of Biomass co-combustion with pulverized coal in a small scale furnace," in *Proceedings of the 6th BSME International Conference on Thermal Engineering, ICTE 2014*, pp. 504–511, Bangladesh, December 2014.

[17] A. Stroh, F. Alobaid, J.-P. Busch, J. Ströhle, and B. Epple, "3-D numerical simulation for co-firing of torrefied biomass in a pulverized-fired 1 MWth combustion chamber," *Energy*, vol. 85, pp. 105–116, 2015.

[18] S. R. Gubba, D. B. Ingham, K. J. Larsen et al., "Numerical modelling of the co-firing of pulverised coal and straw in a 300 MWe tangentially fired boiler," *Fuel Processing Technology*, vol. 104, pp. 181–188, 2012.

[19] C. Ghenai and I. Janajreh, "CFD analysis of the effects of co-firing biomass with coal," *Energy Conversion and Management*, vol. 51, no. 8, pp. 1694–1701, 2010.

[20] J. Li, A. Brzdekiewicz, W. Yang, and W. Blasiak, "Co-firing based on biomass torrefaction in a pulverized coal boiler with aim of 100% fuel switching," *Applied Energy*, vol. 99, pp. 344–354, 2012.

[21] F. Tabet and I. Gökalp, "Review on CFD based models for co-firing coal and biomass," *Renewable & Sustainable Energy Reviews*, vol. 51, pp. 1101–1114, 2015.

[22] A. Gungor, "Simulation of co-firing coal and biomass in circulating fluidized beds," *Energy Conversion and Management*, vol. 65, pp. 574–579, 2013.

[23] X. Zhang, M. Ghamari, and A. Ratner, "Numerical modeling of co-firing a light density biomass, oat (Avena sativa) hulls, and chunk coal in fluidized bed boiler," *Biomass & Bioenergy*, vol. 56, pp. 239–246, 2013.

[24] A. A. Bhuiyan and J. Naser, "CFD modelling of co-firing of biomass with coal under oxy-fuel combustion in a large scale power plant," *Fuel*, vol. 159, pp. 150–168, 2015.

[25] A. A. Bhuiyan and J. Naser, "Computational modelling of co-firing of biomass with coal under oxy-fuel condition in a small scale furnace," *Fuel*, vol. 143, pp. 455–466, 2015.

[26] T. I. Gombosi, *Gaskinetic Theory*, Cambridge University Press, Cambridge, 1994.

[27] M. J. V. Goldschmidt, R. Beetstra, and J. A. M. Kuipers, "Hydrodynamic modelling of dense gas-fluidised beds: Comparison of the kinetic theory of granular flow with 3D hard-sphere discrete particle simulations," *Chemical Engineering Science*, vol. 57, no. 11, pp. 2059–2075, 2002.

[28] C. K. K. Lun, S. B. Savage, D. J. Jeffrey, and N. Chepurniy, "Kinetic theories for granular flow: inelastic particles in Couette flow and slightly inelastic particles in a general flowfield," *Journal of Fluid Mechanics*, vol. 140, pp. 223–256, 1984.

[29] L. Huilin, L. Wenti, B. Rushan, Y. Lidan, and D. Gidaspow, "Kinetic theory of fluidized binary granular mixtures with unequal granular temperature," *Physica A: Statistical Mechanics and its Applications*, vol. 284, no. 1, pp. 265–276, 2000.

[30] L. Huilin, D. Gidaspow, and E. Manger, "Kinetic theory of fluidized binary granular mixtures," *Physical Review E: Statistical, Nonlinear, and Soft Matter Physics*, vol. 64, no. 6 I, pp. 1–8, 2001.

[31] L. Huilin and D. Gidaspow, "Hydrodynamics of binary fluidization in a riser: CFD simulation using two granular temperatures," *Chemical Engineering Science*, vol. 58, no. 16, pp. 3777–3792, 2003.

[32] W. Shuai, C. Juhui, L. Guodong, L. Huilin, Z. Feixiang, and Z. Yanan, "Predictions of coal combustion and desulfurization in a CFB riser reactor by kinetic theory of granular mixture with unequal granular temperature," *Fuel Processing Technology*, vol. 126, pp. 163–172, 2014.

[33] J. Shen, X.-S. Wang, M. Garcia-Perez, D. Mourant, M. J. Rhodes, and C.-Z. Li, "Effects of particle size on the fast pyrolysis of oil mallee woody biomass," *Fuel*, vol. 88, no. 10, pp. 1810–1817, 2009.

[34] W. Fu, Y. Zhang, H. Han, and D. Wang, "A general model of pulverized coal devolatilization," *Fuel*, vol. 68, no. 4, pp. 505–510, 1989.

[35] J. Reina, E. Velo, and L. Puigjaner, "Kinetic study of the pyrolysis of waste wood," *Industrial & Engineering Chemistry Research*, vol. 37, no. 11, pp. 4290–4295, 1998.

[36] E. Desroches-Ducarne, E. Marty, G. Martin, and L. Delfosse', "Co-combustion of coal and municipal solid waste in a circulating fluidized bed," *Fuel*, vol. 77, no. 12, pp. 1311–1315, 1998.

[37] J. B. Howard, G. C. Williams, and D. H. Fine, "Kinetics of carbon monoxide oxidation in postflame gases," *Symposium (International) on Combustion*, vol. 14, no. 1, pp. 975–986, 1973.

[38] S. Chapman, T. G. Cowling, and D. Park, "The Mathematical Theory of Non-Uniform Gases," *American Journal of Physics*, vol. 30, no. 5, pp. 389-389, 1962.

[39] J. M. Heikkinen, B. C. H. Venneker, G. di Nola, W. de Jong, and H. Spliethoff, "CFD simulation and experimental validation of co-combustion of chicken litter and MBM with pulverized coal in a flow reactor," *Fuel Processing Technology*, vol. 89, no. 9, pp. 874–889, 2008.

[40] A. Gungor, "Two-dimensional biomass combustion modeling of CFB," *Fuel*, vol. 87, no. 8-9, pp. 1453–1468, 2008.

[41] J. Adanez, P. Gayán, G. Grasa, L. F. De Diego, L. Armesto, and A. Cabanillas, "Circulating fluidized bed combustion in the turbulent regime: Modelling of carbon combustion efficiency and sulphur retention," *Fuel*, vol. 80, no. 10, pp. 1405–1414, 2001.

[42] Q. Wang, Z. Luo, X. Li, M. Fang, M. Ni, and K. Cen, "A mathematical model for a circulating fluidized bed (CFB) boiler," *Energy*, vol. 24, no. 7, pp. 633–653, 1999.

[43] I. Petersen and J. Werther, "Experimental investigation and modeling of gasification of sewage sludge in the circulating fluidized bed," *Chemical Engineering and Processing: Process Intensification*, vol. 44, no. 7, pp. 717–736, 2005.

[44] I. Matsui, D. Kunii, and T. Furusawa, "Study of char gasification by carbon dioxide. 1. Kinetic study by thermogravimetric analysis," *Industrial & Engineering Chemistry Research*, vol. 26, no. 1, pp. 91–95, 1987.

[45] B. R. Stanmore and P. Gilot, "Review-calcination and carbonation of limestone during thermal cycling for CO2 sequestration," *Fuel Processing Technology*, vol. 86, no. 16, pp. 1707–1743, 2005.

[46] I. Matsui, D. Kunii, and T. Furusawa, "Study of fluidized bed steam gasification of char by thermogravimetrically obtained kinetics," *Journal of Chemical Engineering of Japan*, vol. 18, no. 2, pp. 105–113, 1985.

[47] D. Gidaspow, R. Bezburuah, and J. Ding, "Hydrodynamics of circulating fluidized beds: Kinetic theory approach," in *Proceedings of the 7th international conference on fluidization*, Gold Coast, Australia, May 1992.

[48] D. J. Gunn, "Transfer of heat or mass to particles in fixed and fluidised beds," *International Journal of Heat and Mass Transfer*, vol. 21, no. 4, pp. 467–476, 1978.

[49] K. Myöhänen, T. Hyppänen, J. Miettinen, and R. Parkkonen, "Three-dimensional modeling and model validation of circulating fluidized bed combustion," in *Proceedings of the 17th International Conference on Fluidized Bed Combustion*, pp. 293–303, USA, May 2003.

[50] A. Gungor and N. Eskin, "Two-dimensional coal combustion modeling of CFB," *International Journal of Thermal Sciences*, vol. 47, no. 2, pp. 157–174, 2008.

[51] A. Goyal and A. Rehmat, "Modeling of a fluidized-bed coal carbonizer," *Industrial & Engineering Chemistry Research*, vol. 32, no. 7, pp. 1396–1410, 2002.

[52] W. Zhou, C. Zhao, L. Duan, D. Liu, and X. Chen, "CFD modeling of oxy-coal combustion in circulating fluidized bed," *International Journal of Greenhouse Gas Control*, vol. 5, no. 6, pp. 1489–1497, 2011.

[53] B. Chalermsinsuwan, T. Chanchuey, W. Buakhao, D. Gidaspow, and P. Piumsomboon, "Computational fluid dynamics of circulating fluidized bed downer: Study of modeling parameters and system hydrodynamic characteristics," *Chemical Engineering Journal*, vol. 189-190, pp. 314–335, 2012.

[54] L. Zhao, B. F. Q. Jia, and C. Zhao, "Numerical and experimental study on coal and biomass co-firing in the fluidized bed under O2/CO2 atmospheres," in *Proceedings of the 35th International Symposium on Combustion*, San Francisco, Calif, USA, 2014.